

Image descattering and absorption compensation in underwater polarimetric imaging



Xianping Fu ^{a,b}, Zheng Liang ^{a,*}, Xueyan Ding ^a, Xinyue Yu ^a, Yafei Wang ^a

^a Information Science and Technology School, Dalian Maritime University, Dalian 116026, China

^b Pengcheng Laboratory, Shenzhen, Guangdong 518055, China

ARTICLE INFO

Keywords:

Underwater polarimetric imaging

Image descattering

Absorption compensation

Color correction

ABSTRACT

Underwater image contrast degrades and color distorts due to wavelength attenuation caused by scattering and absorption, and the attenuation rate of different wavelengths is significant different in variety of underwater environment, which leads to the satisfying underwater image restoration very difficult. We propose a novel underwater polarimetric image restoration method that consists of descattering and absorption compensation, which particularly takes into account wavelength- and scenedepth- dependent absorption existed in underwater signal light that is ignored by current polarimetric descattering methods. In the descattering step, an automatic attenuation difference map based background region selection strategy is presented, which can estimate background light without considering the no-object region exists or not. In the absorption compensation step, a novel absorption compensation constraint strategy is introduced into the color restoration algorithm for the detected signal light. The strategy relies on well-preserved color component and an absorption prior constraint. Extensive experiments on real-world underwater images demonstrate that the proposed method is more effective than several previous underwater image restoration or enhancement works.

1. Introduction

In underwater optical imaging, as light travels under water, it suffers from two effects: scattering and absorption. The two effects are caused not only by the watertype itself, but also by other components existing in the water such as dissolved organic matter or small observable floating particles. Scattering effect redirects the orientation of light propagation and brings undesired backscattered light into the optical detector, leading to low contrast and generating a haze that superimposes itself on the image. Absorption effect reduces the energies of signal light according to different wavelengths (namely wavelength-dependent absorption), which makes the image visually generating color distortion such as greenish and bluish. As the imaging distance increase, the two effects becomes more serious. The propagation of light in underwater is shown in Fig. 1.

To tackle these problems, various studies are proposed to restore the degraded underwater image [1–3]. In particular, polarization-based image recovery methods have been widely used to restore the degraded underwater image, which is also used for enhancing the degraded image resulted from the effects of haze [4–6]. Y. Y. Schechner used polarimetric method to restore the degraded underwater image in 2003 [7]. Further researches have been developed to improve this method in

recent years, which demonstrated that polarization-based method is effective for recovering the underwater image. However, as mentioned in our previous work [8], several disadvantages of the previous methods are introduced: (1) Most of the polarization-based methods [9–12] take only the scattering into account without considering the absorption effect. Nevertheless, the absorption effect sometimes is more serious than the scattering effect in underwater situation [13]. (2) To calculate the key parameters always involves in the selection of the background region, recent works often manually or automatically select a region where there exists no object as the background region [14]. However, when there is no above mentioned region can be found, it is limited to estimate the key parameters.

In this paper, we attempt to overcome the aforementioned challenges by designing a novel image descattering and color compensation method in underwater polarimetric imaging. The proposed method robustly restores the degraded underwater images and accurately reconstructs the ground truth colors. We summary the specific contributions as follows:

- We develop a joint image descattering and absorption compensation scheme in underwater polarimetric imaging, which particularly considers the wavelength-dependent absorption of signal light which is neglected in most of previous works.

* Corresponding author.

E-mail addresses: fpx@dltu.edu.cn (X. Fu), zliang@dltu.edu.cn (Z. Liang), dingxueyan@dltu.edu.cn (X. Ding), yuxinyue@dltu.edu.cn (X. Yu), wangyafei@dltu.edu.cn (Y. Wang).

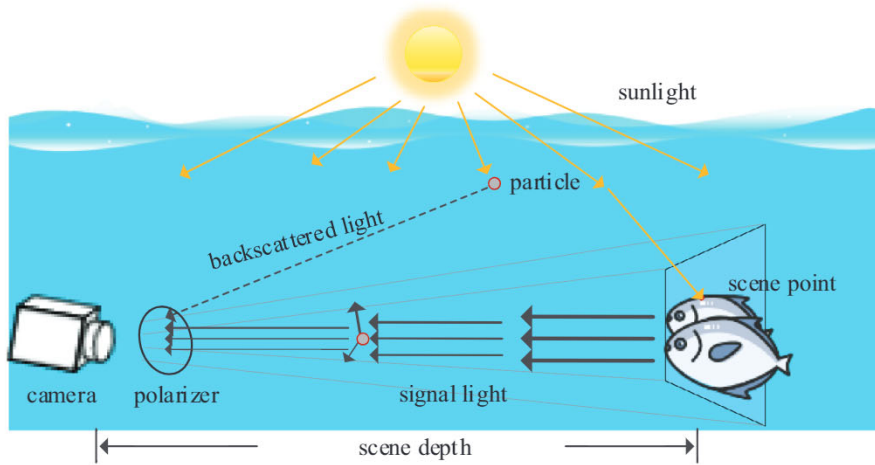


Fig. 1. Underwater imaging degradation model.

- To remove the haze caused by scattering effect, we propose a novel polarimetric descattering method using attenuation difference map-based background region selection strategy that reveals the scene depth information. To the best of our knowledge, it is the first time to provide an automatic method to extract the background region by exploring the light attenuation properties under water.
- We introduce a compensation constraint strategy to restore the color of detected signal light, which relies on the well-preserved color component and an absorption prior. This strategy considers the different wavelengths attenuation level of signal light that caused by wavelength-dependent absorption, thereby generating a better appearance.

2. Optical model of underwater imaging

As depicted in Fig. 1, in underwater imaging, the radiance detected by the camera is composed of two parts: One is the signal light S , whose radiance is attenuated by scattering and wavelength-dependent absorption before finally detected. It can be given by:

$$S(i, j, \lambda) = S_{object}(i, j, \lambda) \exp[-c(\lambda) \cdot z(i, j)], \quad (1)$$

where, S_{object} denotes the signal light without any attenuation, (i, j) is the pixel coordinate, $\lambda = (\lambda_R, \lambda_G, \lambda_B)^T$ indicates the wavelength of the light, z is the distance between the scene object and the camera (namely, scene depth), $c(\lambda)$ is the attenuation coefficient which is the sum of the absorption coefficient $a(\lambda)$ and scattering coefficient $s(\lambda)$ (namely, $c(\lambda) = a(\lambda) + s(\lambda)$).

The other is the backscattered light V that ambient illumination scattered into the camera by suspend particles. It can be given by:

$$V(i, j, \lambda) = V_\infty(\lambda) \{1 - \exp[-s(\lambda) \cdot z(i, j)]\}, \quad (2)$$

where, $V_\infty(\lambda)$ is the backscattered light which extends to infinity. Therefore, the underwater image I captured by the camera can be expressed by:

$$I(i, j) = \int_w I(i, j, \lambda) d\lambda = \int_w [S(i, j, \lambda) + V(i, j, \lambda)] d\lambda, \quad (3)$$

where, w indicates the response waveband of the detector in which a response function $\rho(\lambda)$ indicates the response of the detector to light at each wavelength.

Then, the degraded image can be deduced by:

$$\begin{aligned} I(i, j, \lambda) &= S(i, j, \lambda) + V(i, j, \lambda) \\ &= S_{object}(i, j, \lambda) \exp\{[-a(\lambda) - s(\lambda)] \cdot z(i, j)\} \\ &\quad + V_\infty(\lambda) \{1 - \exp[-s(\lambda) \cdot z(i, j)]\} \\ &= S'_{object}(i, j, \lambda) \exp[-s(\lambda) \cdot z(i, j)] \\ &\quad + V_\infty(\lambda) \{1 - \exp[-s(\lambda) \cdot z(i, j)]\}, \end{aligned} \quad (4)$$

where,

$$S'_{object}(i, j, \lambda) = S_{object}(i, j, \lambda) \exp[-a(\lambda) \cdot z(i, j)]. \quad (5)$$

$S'_{object}(i, j, \lambda)$ denotes the degraded image caused by the absorption effect. Thus, according to Eq. 4 and Eq. 5, the problems caused by the effects of scattering and absorption need to be addressed, respectively. In next section, we describe the details for how we handle these problems.

3. Attenuation difference map based polarimetric descattering method

As mentioned above, scattering changes the orientation of light propagation and brings the undesired backscattered light into the camera, leading to hazy images. In this section, we focus on removing the backscattered light according Eq. (4). The difference between the signal light and backscattered light in polarization behaviors provides a helpful support for removing the backscattered light. In detail, based on the polarization characteristic of light that the backscattered light is partially polarized and the signal light is unpolarized, we propose a novel attenuation difference map based polarimetric descattering method. Before introducing our method, we need to briefly review the traditional polarimetric descattering method.

3.1. Traditional polarimetric descattering method based on two orthogonal polarimetric images

The traditional polarimetric descattering method firstly proposed by Schechner et al. in 2003. In their works, A rotating linear polarizer is mounted in front of the CCD as the analyzer, and through rotating the polarizer, they obtained two polarimetric images at orthogonal states, which are the co-linear image $I^\parallel(i, j, \lambda)$:

$$I^\parallel(i, j, \lambda) = \frac{S(i, j, \lambda)}{2} + V^\parallel(i, j, \lambda), \quad (6)$$

and the cross-linear image $I^\perp(i, j, \lambda)$:

$$I^\perp(i, j, \lambda) = \frac{S(i, j, \lambda)}{2} + V^\perp(i, j, \lambda). \quad (7)$$

Then, the total intensity of the image can be written as:

$$I(i, j, \lambda) = I^\parallel(i, j, \lambda) + I^\perp(i, j, \lambda). \quad (8)$$

The degree of polarization (DoP) of backscattered light $p_V(\lambda)$ and the backscattered light which extends to infinity $V_\infty(\lambda)$ are the two crucial parameters in the polarimetric descattering method, and they can be obtained by:

$$p_V(\lambda) = \frac{1}{|\Theta|} \sum_{(i, j) \in \Theta} \frac{I_\Theta(i, j, \lambda)^\parallel - I_\Theta(i, j, \lambda)^\perp}{I_\Theta(i, j, \lambda)^\parallel + I_\Theta(i, j, \lambda)^\perp}, \quad (9)$$

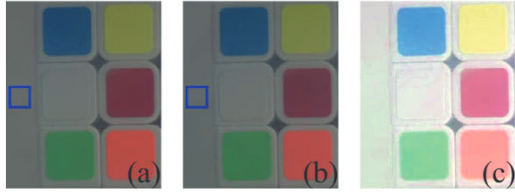


Fig. 2. (a) I^{\parallel} ; (b) I^{\perp} ; (c) Image generated by the traditional polarimetric dehazing method. The blue boxes in (a) and (b) denote the background region. (For interpretation of the references to color in this figure legend, the reader is referred to the web version of this article.)

$$V_{\infty}(\lambda) = \frac{1}{|\Theta|} \sum_{(i,j) \in \Theta} [I_{\Theta}(i,j,\lambda)^{\parallel} + I_{\Theta}(i,j,\lambda)^{\perp}], \quad (10)$$

where, I_{Θ}^{\parallel} and I_{Θ}^{\perp} denote the background region where all the irradiance is contributed by the backscattered light in the image of I^{\parallel} and I^{\perp} , respectively. $|\Theta|$ is the total number of pixels in the background region. The backscattered light can then be estimated by:

$$V(i,j,\lambda) = \frac{I^{\parallel}(i,j,\lambda) - I^{\perp}(i,j,\lambda)}{p_V(\lambda)}, \quad (11)$$

and with Eqs. (1)–(4), the hazy problem caused by the scattering effect can be addressed by:

$$S'_{object} = \frac{I(i,j,\lambda) - V(i,j,\lambda)}{1 - [V(i,j,\lambda)/V_{\infty}(\lambda)]}. \quad (12)$$

Two orthogonal polarimetric images and dehazed image generated by the traditional method are presented in Fig. 2(a)–(c), respectively. We can obviously see that visibility of the image generated by the traditional method is poor, there are two reasons for it: Firstly, it is difficult to acquire the two orthogonal polarimetric images in the same scene because of the rapid changes of the scene structure and light illumination conditions. Secondly, the precise selection of the region where the object does not exist is crucial for the estimation of $p_V(\lambda)$ and $V_{\infty}(\lambda)$, which is difficult to implement automatically.

3.2. Attenuation difference map based polarimetric descattering method

Two orthogonal polarimetric images I^{\parallel} and I^{\perp} are employed to estimate the desired parameters in several previous works. But it is arduous to accurately acquire the two orthogonal polarimetric images. To avoid this, the Stokes parameters-based polarimetric algorithm method is proposed in our method. A rotating linear polarizer is mounted in front of the CCD as the analyzer, and through rotating the polarizer's angle to be $0^\circ, 45^\circ, 90^\circ$, we can get three different polarimetric images $I_0(i,j,\lambda)$, $I_{45}(i,j,\lambda)$, $I_{90}(i,j,\lambda)$. The stokes parameters can be written as:

$$\begin{aligned} I(i,j,\lambda) &= I_0(i,j,\lambda) + I_{90}(i,j,\lambda), \\ Q(i,j,\lambda) &= I_0(i,j,\lambda) - I_{90}(i,j,\lambda), \\ U(i,j,\lambda) &= 2I_{45}(i,j,\lambda) - I(i,j,\lambda), \end{aligned} \quad (13)$$

where, I represents the total intensity of light detected by the camera, Q and U represent the intensity information of the linear polarization state.

The key point of polarimetric image recovery is estimating the DoP of the backscattered light and the backscattered light which extends to infinity. As depicted in Section 3.1, they can be estimated from those pixels in the background region. However, the background region needs to be marked out manually in the previous works, which may affect the precise of parameters estimation. In addition, considering the fact that the demands for dehazing techniques are generally in real underwater applications. An effective method which can extract the background region automatically is meaningful, and thus desired.

From Eqs. (4) and (5), all the wavelengths are gradually absorbed with the increase of scene depth, and eventually all the irradiance is

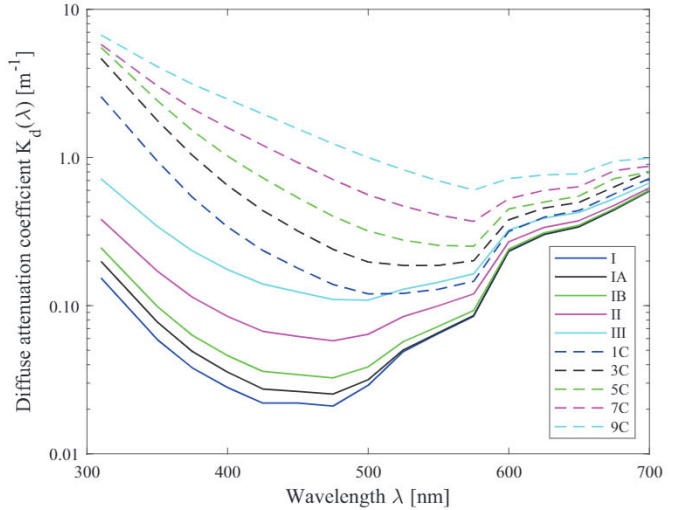


Fig. 3. Diffuse attenuation coefficients $K_d(\lambda)$ of Jerlov water types from [15]. Solid lines mark open ocean water types (I through III) while dashed lines mark coastal water types (1C through 9C). For open ocean waters, Type-I is the clearest and Type-III is the most turbid. Similarly, Type-1C is the clearest coastal water and Type-9C is the most turbid.

contributed only by the backscattered light. For example, when $z(i,j) \rightarrow \infty$, $\exp[-a(\lambda) \cdot z(i,j)] \rightarrow 0$ and $\{1 - \exp[-s(\lambda) \cdot z(i,j)]\} \rightarrow 1$. Therefore, strictly speaking, the selection of the background region depends on the scene depth.

As shown in Fig. 3, the attenuation rate between different wavelengths under water is significantly different due to the wavelength-dependent absorption, which provides an important support for estimating the attenuation difference map that reflect the scene depth information. We first simply use the difference (namely, attenuation map $M(i,j,\lambda)$) between the original intensity and the intensity received by camera to assess the attenuation level of each color wavelength light. It is mathematically represented as:

$$M(i,j,\lambda) = 1 - I^{\gamma}(i,j,\lambda). \quad (14)$$

To satisfy the observation characteristics of human eyes, where gamma correction is utilized to correct the received light intensity (we generate our results with the default value of $\gamma = 1.2$). Then, the color wavelength that attenuates at the highest rate under water can be selected by:

$$\lambda_{c^*} = \arg \max_{c|c \in \{R,G,B\}} \frac{\iint M(i,j,\lambda_c) di dj}{\iint di dj}. \quad (15)$$

Next, the attenuation difference map can be estimated based on the significant difference between different wavelength in the attenuation rate by:

$$D(i,j) = \max_{(i,j) \in \Omega} I(i,j,\lambda_{c^*}) - \max_{(i,j) \in \Omega} I(i,j,\lambda'_{c'}), \quad (16)$$

where, Ω refers to a patch in the image, λ_{c^*} indicates the color wavelength that attenuates at the highest rate and $\lambda'_{c'}$ denotes the other color wavelengths. Large values of $D(i,j)$ represent closer scene points. After the attenuation difference map is obtained, we select the farthest 0.1% of pixels as these pixels in the background region (the background region is defined as Δ). With the help of these pixels, the $p_V(\lambda)$ and $\theta_V(\lambda)$ can be obtained by:

$$p_V(\lambda) = \frac{1}{|\Delta|} \sum_{(i,j) \in \Delta} \frac{\sqrt{Q^2(i,j,\lambda) + U^2(i,j,\lambda)}}{I(i,j,\lambda)}, \quad (17)$$

and

$$\theta_V(\lambda) = \frac{1}{2|\Delta|} \sum_{(i,j) \in \Delta} \arctan \left[\frac{U(i,j,\lambda)}{Q(i,j,\lambda)} \right], \quad (18)$$

where, $\theta_V(\lambda)$ is the angle of polarization (AoP) of the backscattered light. $|\Delta|$ indicates the total number of pixels in the area at infinity. In addition, the $V_\infty(\lambda)$ can also be estimated from these pixels by:

$$V_\infty(\lambda) = I(i^*, j^*, \lambda) \text{ with} \\ (i^*, j^*) = \arg \max_{(i,j)|D(i,j) < D^{99.9}} [I(i, j, \lambda_R) + I(i, j, \lambda_G) + I(i, j, \lambda_B)], \quad (19)$$

where, (i^*, j^*) denotes the location of the brightest pixel among those pixels whose scene depth value lies below the 99.9th percentile $D^{99.9}$. According to the value of $p_{V(\lambda)}$ and $\theta_{V(\lambda)}$, the backscattered light is obtained by:

$$V(i, j, \lambda) = \frac{I_0 - I[1 - p(\lambda)]/2}{p_V(\lambda) \cdot \cos^2 \theta_V(\lambda)} = \frac{I_{90} - I[1 - p(\lambda)]/2}{p_V(\lambda) \cdot \sin^2 \theta_V(\lambda)}, \quad (20)$$

where,

$$p(\lambda) = \frac{\sqrt{Q^2(i, j, \lambda) + U^2(i, j, \lambda)}}{I(i, j, \lambda)}, \quad (21)$$

is the DoP of the total radiance of the backscattered light and the signal light over the whole image. After measuring $p_{V(\lambda)}$, to avoid the influence of noise, we slightly increase it using the operation $p_{V(\lambda)} \rightarrow \epsilon p_{V(\lambda)}$, where $1 \leq \epsilon \leq 1/p_{V(\lambda)}$, before using $p_{V(\lambda)}$ in Eq. 20 with Eqs. (4)–(21), the backscattered light caused by the scattering effect under water can be removed by:

$$S'_{\text{object}}(i, j, \lambda) = S_{\text{object}}(i, j, \lambda) \exp[-\mathbf{a}(\lambda) \cdot \mathbf{z}(i, j)] \\ = \frac{I(i, j, \lambda) - V(i, j, \lambda)}{1 - [V(i, j, \lambda)/V_\infty(\lambda)]}. \quad (22)$$

4. Absorption compensation using a novel color correction method

In the above step, the attenuation difference map based polarimetric descattering method works well in removing the backscattered light, but unfortunately, it can not compensate for the color shift caused by the wavelength-dependent absorption under water. Therefore, the next work mainly focus on correcting the problem of underwater image color shift by a novel color correction method.

The proposed correction method is based on the [16]. In [16], the authors think that the green color component can be well preserved under water and use the information of the green component to compensate for the other two color components. Mathematically, it is express as:

$$S_{\text{object}}(i, j, \lambda_R) = S'_{\text{object}}(i, j, \lambda_R) + \alpha_1 \left[\frac{\iint S'_{\text{object}}(i, j, \lambda_G) djdj}{\iint didj} \right. \\ \left. - \frac{\iint S'_{\text{object}}(i, j, \lambda_R) djdj}{\iint didj} \right] \left[1 - S'_{\text{object}}(i, j, \lambda_R) \right] S'_{\text{object}}(i, j, \lambda_G) \quad (23)$$

and

$$S_{\text{object}}(i, j, \lambda_B) = S'_{\text{object}}(i, j, \lambda_B) + \alpha_2 \left[\frac{\iint S'_{\text{object}}(i, j, \lambda_G) djdj}{\iint didj} \right. \\ \left. - \frac{\iint S'_{\text{object}}(i, j, \lambda_B) djdj}{\iint didj} \right] \left[1 - S'_{\text{object}}(i, j, \lambda_B) \right] S'_{\text{object}}(i, j, \lambda_G) \quad (24)$$

where $S_{\text{object}}(i, j, \lambda_R)$, $S_{\text{object}}(i, j, \lambda_B)$ denote the compensated red and blue component, $S'_{\text{object}}(i, j, \lambda_R)$ and $S'_{\text{object}}(i, j, \lambda_B)$ represent the red and blue component that needs to be compensated, and α_1 and α_2 indicate two constant parameters. However, it should be noted that the green component only preserves better in some conditions, not in all. In clear seawater, most images are in green-bluish appearance, but for turbid water, red component or even near-infrared component may propagate longer [13]. It is not feasible to choose green component as the reference for all water conditions.

In the proposed method, we can first find that which one can be well preserved under water in R, G, B three color component using the attenuation map. After the well-preserved color component is determined, it can be used as a bias to compensate for the other two color components. Secondly, we compensate for the other two color light intensity information by adding a fraction of the well-preserved color component

light intensity information. Since the reason of color cast is that the absorption coefficient between the different wavelength of light has significant difference [17], the other two color components compensation should be proportional to absorption coefficient ratios. For instance, if it is found that the green color component can be well preserved, the red or blue color component compensation should be proportional to the red-green absorption coefficient ratio and blue-green absorption coefficient. So how to obtain the two ratios? Inspired by [18] and [7], the relationship between the backscattered light which extends to infinity $V_\infty(\lambda)$ and the attenuation coefficient $c(\lambda)$ can be obtained by:

$$V_\infty(\lambda) = \frac{k_l E_a}{c(\lambda)} \int_\theta \xi(\lambda, \varphi) d\varphi, \quad (25)$$

where, φ is the scattering angle relative to the propagation direction, θ indicates all possible scattering angles for a certain scattering volume, $\xi(\lambda, \varphi)$ represents a response function in the volume, E_a denotes the intensity of the ambient light that is simplified to a constant, k_l indicates the parameter about the properties of the detector and is a constant. $\int_\theta \xi(\lambda, \varphi) d\varphi$ represents all scattering accidents toward the detector from all angles and is essentially identical with the definition of scattering coefficient $s(\lambda)$. Then it can be derived as:

$$V_\infty(\lambda) \propto \frac{s(\lambda)}{c(\lambda)}. \quad (26)$$

Eq. (26) implies that the backscattered light which extends to infinity $V_\infty(\lambda)$ is proportional to the scattering coefficient and inversely proportional to the attenuation coefficient $c(\lambda)$. Based on the fact that the attenuation of the image after descattering almost entirely comes from the wavelength-dependent absorption, an approximation is made that the attenuation coefficient is equal to absorption coefficient (namely, $c(\lambda) \rightarrow a(\lambda)$). Eq. (26) can be further deduced roughly as [19]:

$$V'_\infty(\lambda) \propto \frac{s(\lambda)}{a(\lambda)}. \quad (27)$$

where $V'_\infty(\lambda)$ is the backscatterend light which extends to infinity in the descattered image, and similar to Eq. (19), it can be derived by:

$$V'_\infty(\lambda) = S'_{\text{object}}(i^*, j^*, \lambda) \text{ with} \\ (i^*, j^*) = \arg \max_{(i,j)|D(i,j) < D^{99.9}} [S'_{\text{object}}(i, j, \lambda_R) + S'_{\text{object}}(i, j, \lambda_G) + S'_{\text{object}}(i, j, \lambda_B)], \quad (28)$$

where, (i^*, j^*) denotes the location of the brightest pixel among those pixels whose scene depth value lies below the 99.9th percentile $D^{99.9}$.

Gould et al. [20] found the approximately linear relationship between the scattering coefficient and wavelength of light, as following:

$$s(\lambda) = (-0.00113\lambda + 1.62517)\tau(\lambda), \quad (29)$$

where, $\tau(\lambda)$ can be simplified to an identical value in each color component.

According to Eqs. (27) and (29), we can obtain a prior about absorption ratios, it can be expressed as:

$$\frac{a(\lambda_R)}{a(\lambda_G)} = \frac{s(\lambda_R)V'_\infty(\lambda_G)}{s(\lambda_G)V'_\infty(\lambda_R)} \\ = \frac{(-0.00113\lambda_R + 1.62517)V'_\infty(\lambda_G)}{(-0.00113\lambda_G + 1.62517)V'_\infty(\lambda_R)}, \quad (30)$$

$$\frac{a(\lambda_B)}{a(\lambda_G)} = \frac{s(\lambda_B)V'_\infty(\lambda_B)}{s(\lambda_G)V'_\infty(\lambda_B)} \\ = \frac{(-0.00113\lambda_B + 1.62517)V'_\infty(\lambda_B)}{(-0.00113\lambda_G + 1.62517)V'_\infty(\lambda_B)}, \quad (31)$$

where, λ_R , λ_G , λ_B denotes the wavelength of the red, green, and blue components ($\lambda_R = 620\text{nm}$, $\lambda_G = 540\text{nm}$, $\lambda_B = 450\text{nm}$ under water). $V_\infty(\lambda_R)$, $V_\infty(\lambda_G)$, $V_\infty(\lambda_B)$ are the backscattered light intensity of different color wavelength which extends to infinity, they can be derived from Eq. (28). Finally, based on the Gray-World assumption that all color components have the same mean value before attenuation, the proposed

color compensation method can be written as:

$$S_{\text{object}}(i, j, \lambda_c) = S'_{\text{object}}(i, j, \lambda_c) + \left[\frac{\int \int S'_{\text{object}}(i, j, \lambda_c'') didj}{\int \int didj} \right] \left[\frac{a(\lambda_c)}{a(\lambda_c'')} + \eta \right] S'_{\text{object}}(i, j, \lambda_c''), \quad (32)$$

where, $S'_{\text{object}}(i, j, \lambda_c)$ is the color component that needs to be compensated in the descattered image, $S'_{\text{object}}(i, j, \lambda_c'')$ indicates the well-preserved color component. η is an adaptive parameters to control the strength of wavelength compensation.

5. Experiment and discussion

To assess the validation of the proposed method, we conduct real-world underwater polarimetric image restoration experiments. In our experiments, an 8 bit digital COMS camera (Nikon D5300) is used as the imaging device under natural illumination. A rotating linear polarizer is mounted in front of the camera. To simulate the effects of the scattering and absorption under water, we poured the milk and color ink into a $50\text{cm} \times 50\text{cm} \times 50\text{cm}$ water tank. A rough-surface plastic Rubik's cube and a bottle are chosen as two targets, three raw polarimetric images with the polarizer at the angle of 0° , 45° , 90° can be obtained through rotating the polarizer to different directions. Fig. 4 shows the schematic diagram of proposed image recovery method.

5.1. Qualitative result

The raw images and the restored results generated by different process are shown in Figs. 5 and 6. Besides, the images taken in clear water are also presented in Figs. 5 and 6 for comparison. It can be found that the proposed attenuation difference map based polarimetric decattering method can effectively remove the haze caused by the scattering effect, but the images still suffer from color cast. With the help of color compensation (the parameter η is set to zero in our experiments), the colors are significantly restored and close to those in the clear water image. To further assess the results of image recovery in more detail, we use RGB spatial coordinate systems to depict the pixel distribution of the R, G and B color component. It can be seen that the pixels have more dispersed distribution in these images generated by the proposed method, which is more similar to the RGB of in clear water image.

Additionally, we compared it with three previous works: Schechner method [7], UDCP [21] and Retinex [22]. As shown in Fig. 7, the effects of scattering and absorption can be successfully removed by our algorithm and the visibility of underwater images is effectively restored. Although the qualitative comparison also demonstrate that other methods mentioned above are able to achieve better enhancement for underwater hazy images, but due to the accurate estimation of these significant parameters in our method and the outperform of the color correction, the results of the proposed method are more natural than the results of other methods. As we can see in Fig. 7, the performance of the Schechner method is the worst among these methods, which may be related to our failure to correctly select the region at infinity. the results of UDCP

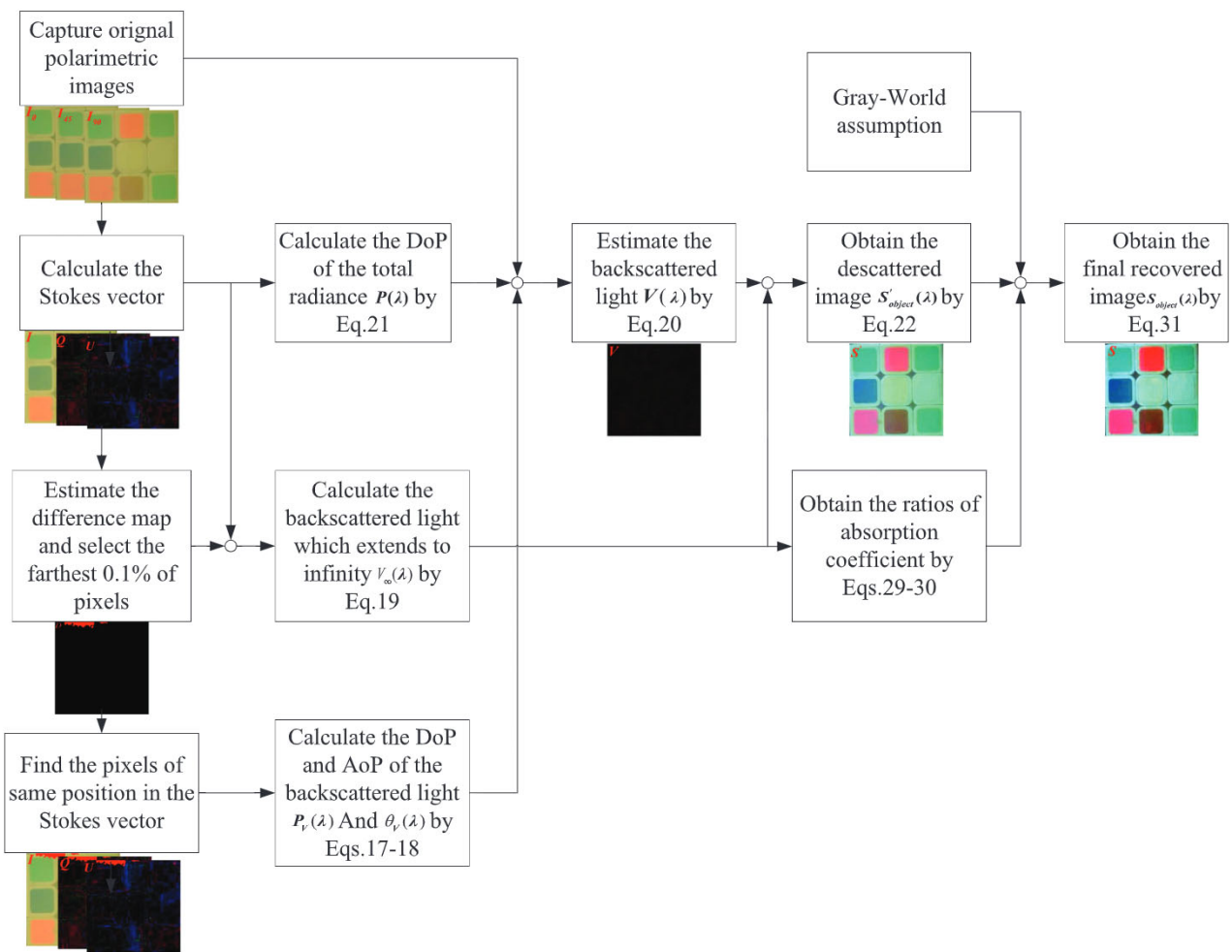


Fig. 4. The flowchart of image descattering and color compensation in underwater polarimetric imaging.

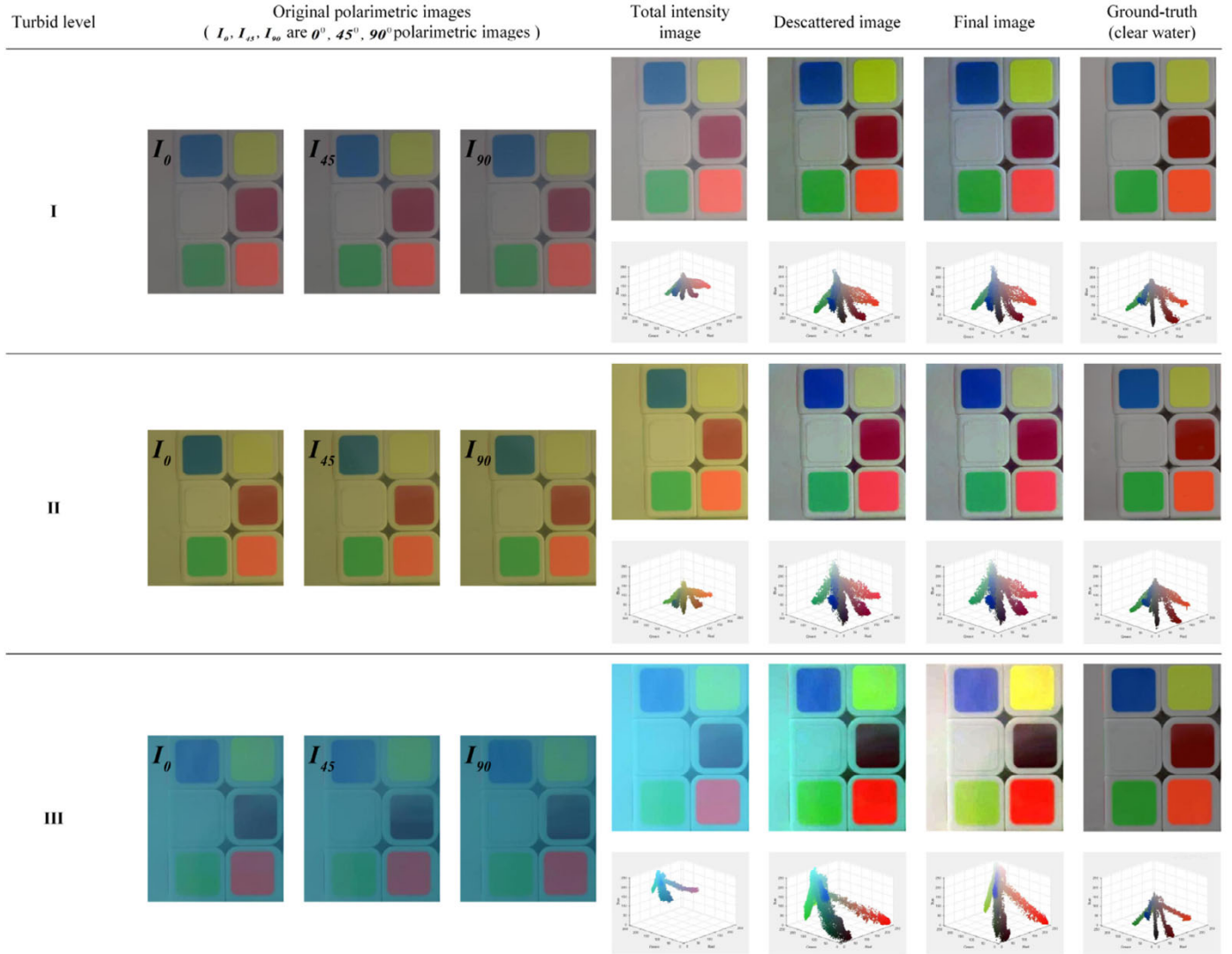


Fig. 5. The raw images taken under different water types and the result generated by different process. From left to right are underwater environments with different turbid level (Turbid level I is made only by milk, Turbid level II is made by milk and yellow ink, and turbid level III is made by milk and blue ink.), the original polarimetric image taken under different polarizer directions, the total intensity image, the descattered image yielded by the attenuation difference map based polarimetric image descattering method, the final restored image with absorption compensation and the image in clear water. (For interpretation of the references to color in this figure legend, the reader is referred to the web version of this article.)

method generally look darker, and also have color distortion. Retinex method although can make more satisfactory dehazed results, but unfortunately, the color of the enhanced image looks particularly weird, and the details are not good enough.

Here, the practical application of the proposed method is verified. As shown in Fig. 8, more practical enhancement results are carried out for real-world underwater hazy images captured in two small ponds. It should be noted that it is difficult to find a region where there exists no object in Fig. 8, which leads most previous works that relies on the region to difficultly restore, but it can be found that the proposed method is effective for these underwater images.

5.2. Quantitative result

Since the ground truth images are available in the Fig. 7, we compare it against the previous underwater image enhancement or restoration works via three full-reference underwater quality evaluation metrics: MSE (mean square error) [23], PSNR (peak signal-to-noise ratio) [24], SSIM (structural similarity index measure) [24]. The MSE metric is the most widely used and also the simplest, which is calculated by the

squared intensity differences of restored and reference image pixels,

$$\text{MSE} = \frac{1}{H \times W \times C} \sum_{i=1}^H \sum_{j=1}^W \sum_{k=1}^C (S_{\text{res}}(i, j, k) - S_{\text{ref}}(i, j, k))^2 \quad (33)$$

where, H , W , and C indicate the width, height and channel in the image size, respectively. $S_{\text{res}}(i, j, k)$ is the pixel value at the position (i, j, k) in the restored color image S_{res} , and $S_{\text{ref}}(i, j, k)$ is the pixel value at the position (i, j, k) in the reference color image S_{ref} , here we use the image in clear water (ground-truth) as the reference image. The lower value of the MSE stands for the better performance. PSNR is generally used to assess the color similarity between the restored image and the reference image, it can be expressed by,

$$\text{PSNR} = 10 \cdot \log_{10} \left(\frac{\text{MAX}^2}{\text{MSE}} \right) \quad (34)$$

where the MAX denotes the possible maximum value of the image, and is equal to 255 in most cases. The higher PSNR value indicates the result is closer to the reference image in terms of image color. In addition, we use SSIM metric to evaluate the structural similarity between the restored image and the reference image, the higher SSIM scores mean

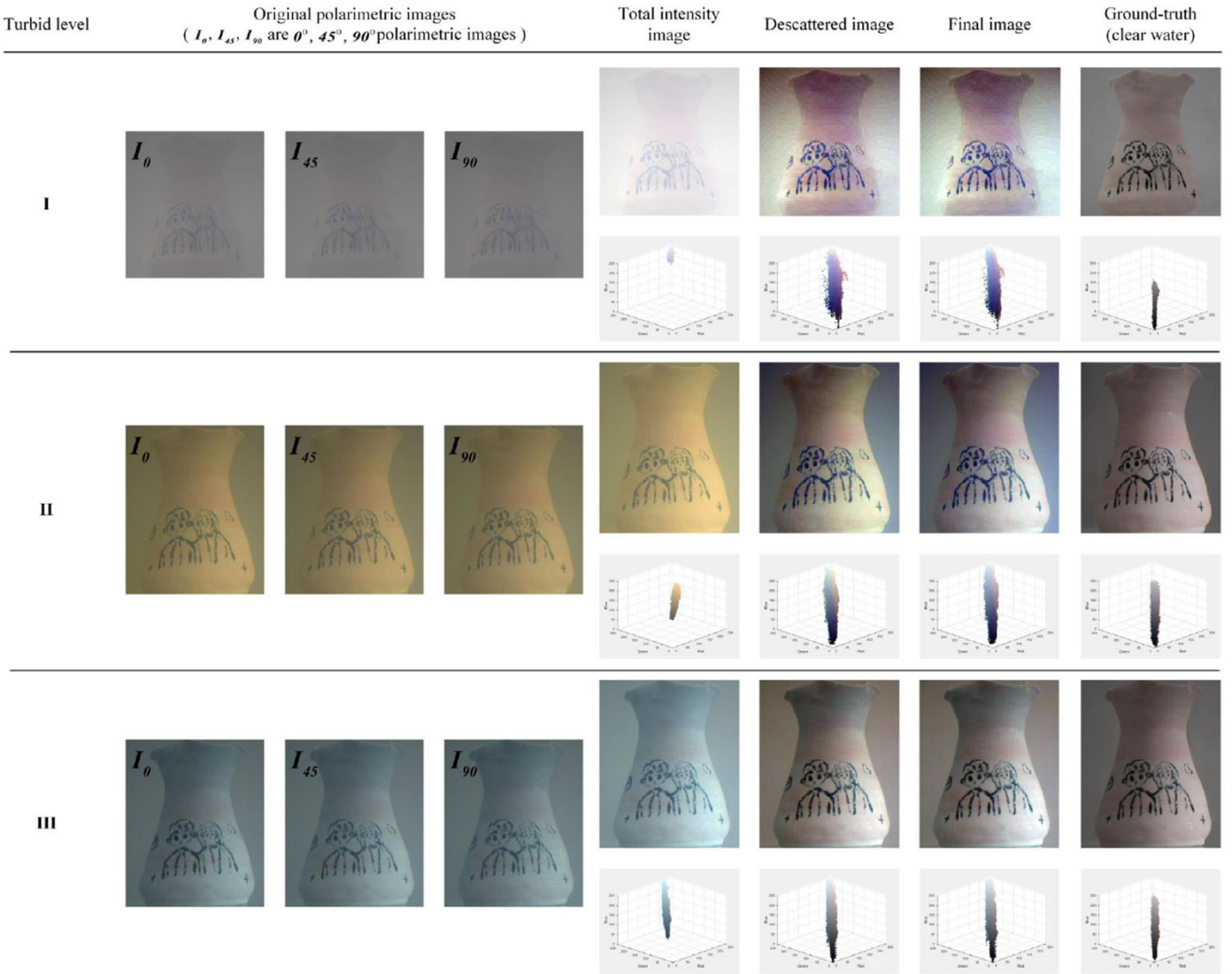


Fig. 6. The raw images taken under different water types and the result generated by different process.

Table 1
Quantitative MSE, PSNR and SSIM values of samples in Fig. 7.

Assessments	Methods	Fig. 7(a)	Fig. 7(b)	Fig. 7(c)	Fig. 7(d)	Fig. 7(e)	Fig. 7(f)
MSE	Schechner	7.2137	1.7177	5.8070	4.9467	4.1330	4.0723
	UDCP	1.3875	1.6286	2.2099	3.7714	2.7221	2.5760
	Retinex	1.6511	1.9453	2.0699	2.9464	1.1557	1.1874
	Ours	0.1984	0.5863	5.9682	3.2527	0.9799	0.9693
PSNR	Schechner	9.5492	15.7814	10.4913	11.1876	11.9681	12.0324
	UDCP	16.7084	16.0127	14.6870	12.3658	13.7818	14.0214
	Retinex	15.9532	15.2409	14.9714	13.4378	17.5025	17.3848
	Ours	25.1542	20.4495	10.3724	13.0084	18.2186	18.2659
SSIM	Schechner	0.6794	0.4298	0.1074	0.5299	0.2912	0.0275
	UDCP	0.6214	0.4556	0.3034	0.4747	0.1871	0.1015
	Retinex	0.5338	0.5338	0.5298	0.5186	0.6474	0.6598
	Ours	0.6808	0.6985	0.6292	0.6024	0.6046	0.7451

the restored image is more similar to the reference image in terms of image structure and texture.

Table 1 calculates the evaluation values of the challenging results that are shown in Fig. 7, the values in bold represent the best results. As visible, among these comparable underwater image restoration methods we tested, the proposed method performs better in terms of the values

MSE and PSNR except for Fig. 7 (c) and (d), but our method visually generates better results with no block effects for Fig. 7 (c) and (d). Our method significantly improves the SSIM values comparing with other methods.

To further quantitatively demonstrate the advantages processed by the proposed method, three no-reference evaluation metrics are em-

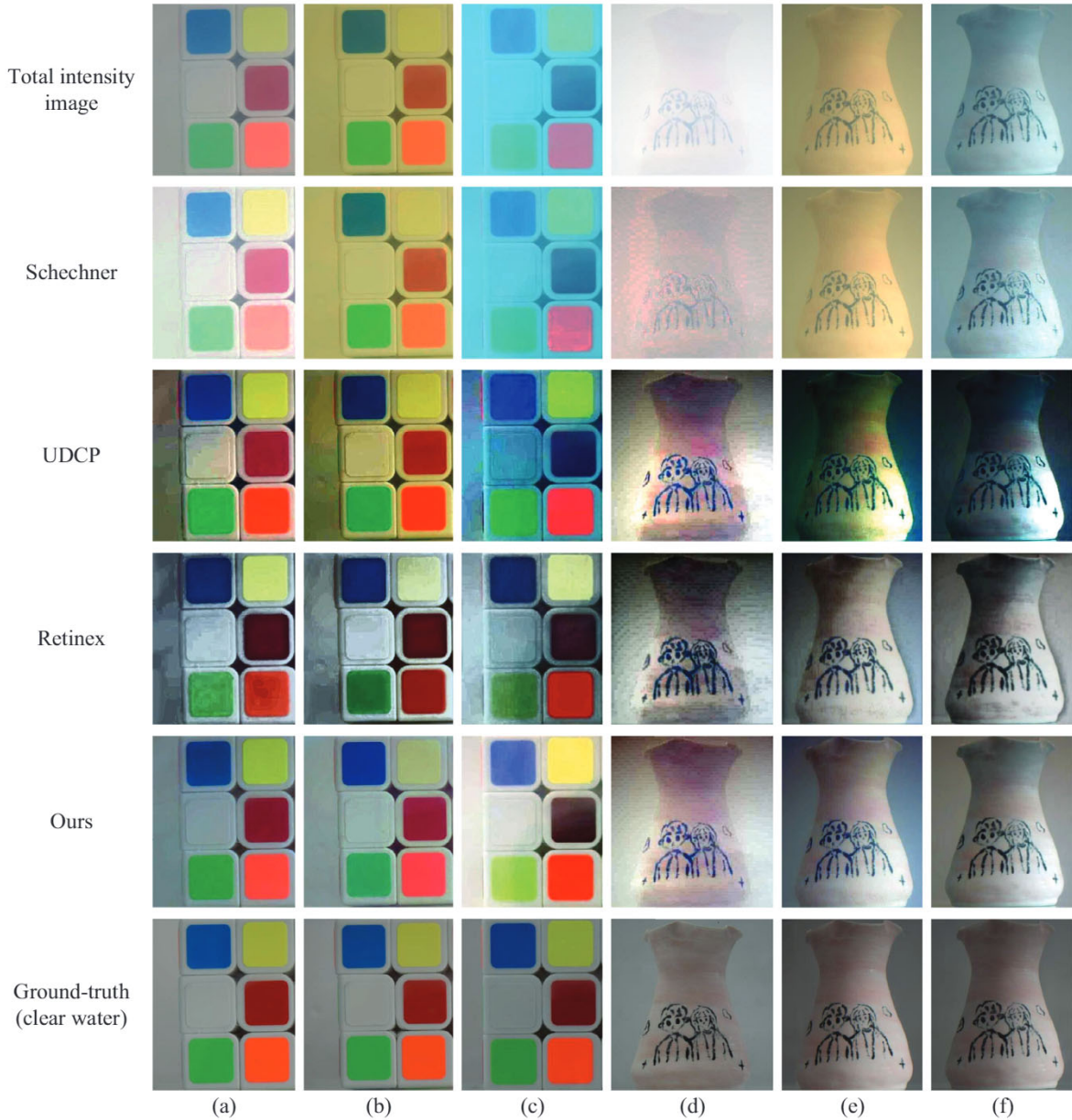


Fig. 7. The restored results generated among different underwater image enhancement methods. (a)–(f) denote different samples taken in various turbid underwater environments. The first row is the total intensity image, the second row to the last row are the results generated by Schechner, UDCP, Retinex, the proposed method and Ground-truth, respectively.

ployed for underwater images presented in Fig. 8. Entropy [25] is a measure of the richness of details of the image, and the highest score means that the method can produce the most visually appealing results with more information content. UIQM (underwater image quality measure) [26] evaluates the quality of an underwater image by its sharpness measure, colorfulness measure and contrast measure, and the higher value of the UIQM stands for the better performance. UCIQE (underwater color image quality evaluation) [27] is also served as objective evaluation. The highest UCIQE value indicates the image has a better balance among chroma, saturation, and contrast. Table 2 presents the measurement values, and the values in bold indicate the best results. It can be found that the proposed method stands out among these compared methods.

Overall, we conclude that our approach generally results in better perceptual, with sufficient restoration of the color and the structure.

Table 2
Quantitative Entropy, UIQM and UCIQE values of samples in Fig. 8.

Assessments	Methods	Fig. 8(a)	Fig. 8(b)
Entropy	Schechner	6.1967	5.0519
	UDCP	7.6765	6.9146
	Retinex	7.3353	7.6529
	Ours	7.6826	7.7439
UIQM	Schechner	0.6077	0.4045
	UDCP	1.2303	1.0933
	Retinex	1.2237	1.3348
UCIQE	Ours	1.2330	1.2741
	Schechner	0.3126	0.2541
	UDCP	0.5822	0.5152
	Retinex	0.5462	0.5624
	Ours	0.6198	0.6089



Fig. 8. More practical results on underwater images captured in real underwater environment. (a) and (b) are two real-world underwater images captured in two small ponds. The first column is the total intensity image, the second column to the last column are the results generated by Schechner, UDCP, Retinex and the proposed method, respectively.

6. Conclusion

In this paper, a new scheme that combines image descattering and absorption compensation is proposed to restore the visibility of images taken in turbid water, and it is proven to be effective. The contributions of this paper can be summarized into three points. First, we develop a joint image descattering and absorption compensation scheme in underwater polarimetric imaging, which particularly considers the wavelength-dependent absorption existed in signal light which are neglected in most of the previous works. Second, a novel attenuation difference map based polarimetric descattering method is proposed to remove the haze caused by the scattering effect. In our method, the background region can be extracted automatically based on the attenuation difference map, which can ensure the accuracy of parameters estimation. To our best knowledge, it is the first time to provide a automatic method to extract the background region by exploring the light attenuation properties under water, which further improves the practicability of the proposed method. Furthermore, a compensation constraint strategy is proposed to compensate for the color cast resulting from wavelength-absorption, which relies on well-preserved color component and an absorption prior. The experiments verify that the scheme performs well in enhancing the visibility of underwater images, and even better than other underwater image enhancement methods.

Declaration of Competing Interest

The authors declare that they have no known competing financial interests or personal relationships that could have appeared to influence the work reported in this paper.

CRediT authorship contribution statement

Xianping Fu: Writing - review & editing, Supervision, Project administration, Funding acquisition. **Zheng Liang:** Writing - original draft, Writing - review & editing, Conceptualization. **Xueyan Ding:** Software. **Xinyue Yu:** Validation, Investigation. **Yafei Wang:** Writing - original draft, Writing - review & editing, Conceptualization.

Acknowledgment

The authors would like to thank Peng Lin for his scientific collaboration in this research work. The authors sincerely thank the editors and anonymous reviewers for the very helpful and kind

comments to assist in improving the presentation of our paper. This work was supported in part by the National Natural Science Foundation of China Grant 61802043, Grant 61370142 and Grant 61272368, by the Fundamental Research Funds for the Central Universities Grant 3132019203, Grant 3132016352, by the Dalian Science and Technology Innovation Fund 2018J12GX037 and Dalian Leading Talent Grant, by the Foundation of Liaoning Key Research and Development Program.

References

- [1] Chiang JY, Chen Y-C. Underwater image enhancement by wavelength compensation and dehazing. *IEEE Trans Image Process* 2011;21(4):1756–69.
- [2] Lu J, Li N, Zhang S, Yu Z, Zheng H, Zheng B. Multi-scale adversarial network for underwater image restoration. *Opt Laser Technol* 2019;110:105–13.
- [3] Zhou Y, Wu Q, Yan K, Feng L, Xiang W. Underwater image restoration using color-line model. *IEEE Trans Circuits Syst Video Techno* 2018;29(3):907–11.
- [4] Fang S, Xia X, Huo X, Chen C. Image dehazing using polarization effects of objects and airlight. *Opt Express* 2014;22(16):19523–37.
- [5] Liang J, Ren L, Ju H, Zhang W, Qu E. Polarimetric dehazing method for dense haze removal based on distribution analysis of angle of polarization. *Opt Express* 2015;23(20):26146–57.
- [6] Zhang W, Liang J, Ju H, Ren L, Qu E, Wu Z. A robust haze-removal scheme in polarimetric dehazing imaging based on automatic identification of sky region. *Opt Laser Technol* 2016;86:145–51.
- [7] Schechner YY, Karpel N. Clear underwater vision. In: Proceedings of the 2004 IEEE computer society conference on computer vision and pattern recognition (CVPR); 2004. I–I
- [8] Liang Z, Zhao C, Wang Y, Ding X, Mi Z, Fu X. Adaptive underwater image recovery using polarimetric imaging. In: 2018 international conference on graphics and image processing (ICGIP); 2019. p. 110692L.
- [9] Huang B, Liu T, Hu H, Han J, Yu M. Underwater image recovery considering polarization effects of objects. *Opt Express* 2016;24(9):9826–38.
- [10] Hu H, Zhao L, Huang B, Li X, Wang H, Liu T. Enhancing visibility of polarimetric underwater image by transmittance correction. *IEEE Photonics J* 2017;9(3):1–10.
- [11] Hu H, Zhao L, Li X, Wang H, Yang J, Li K, et al. Polarimetric image recovery in turbid media employing circularly polarized light. *Opt Express* 2018;26(19):25047–59.
- [12] Yang L, Liang J, Zhang W, Ju H, Ren L, Shao X. Underwater polarimetric imaging for visibility enhancement utilizing active unpolarized illumination. *Opt Commun* 2019;438:96–101.
- [13] Akkaynak D, Treibitz T. A revised underwater image formation model. In: Proceedings of the 2018 IEEE computer society conference on computer vision and pattern recognition (CVPR); 2018. p. 6723–32.
- [14] Liu T, Guan Z, Li X, Cheng Z, Han Y, Yang J, et al. Polarimetric underwater image recovery for color image with crosstalk compensation. *Opt Lasers Eng* 2020;124:105833.
- [15] Jerlov N. Irradiance optical classification. *Opt Oceanogr* 1968:118–20.
- [16] Ancuti CO, Ancuti C, De Vleeschouwer C, Bekkert P. Color balance and fusion for underwater image enhancement. *IEEE Trans Image Process* 2017;27(1):379–93.
- [17] Zhang W, Li G, Ying Z. A new underwater image enhancing method via color correction and illumination adjustment. In: 2017 IEEE visual communications and image processing (VCIP). IEEE; 2017. p. 1–4.
- [18] Zhao X, Jin T, Qu S. Deriving inherent optical properties from background color and underwater image enhancement. *Ocean Eng* 2015;94:163–72.

- [19] Liu F, Wei Y, Han P, Yang K, Bai L, Shao X. Polarization-based exploration for clear underwater vision in natural illumination. *Opt Express* 2019;27(3):3629–41.
- [20] Gould RW, Arnone RA, Martinolich PM. Spectral dependence of the scattering coefficient in case 1 and case 2 waters. *Appl Opt* 1999;38(12):2377–83.
- [21] Drews P, Nascimento E, Moraes F, Botelho S, Campos M. Transmission estimation in underwater single images. In: Proceedings of the IEEE international conference on computer vision workshops (ICCVW); 2013. p. 825–30.
- [22] Fu X, Zhuang P, Huang Y, Liao Y, Zhang X-P, Ding X. A retinex-based enhancing approach for single underwater image. In: 2014 IEEE international conference on image processing (ICIP). IEEE; 2014. p. 4572–6.
- [23] Sara U, Akter M, Uddin MS. Image quality assessment through fsim, ssim, mse and psnr—a comparative study. *J Comput Commun* 2019;7(3):8–18.
- [24] Li C, Anwar S, Porikli F. Underwater scene prior inspired deep underwater image and video enhancement. *Pattern Recognit* 2020;98:107038.
- [25] Singh K, Kapoor R. Image enhancement using exposure based sub image histogram equalization. *Pattern Recognit Lett* 2014;36:10–14.
- [26] Panetta K, Gao C, Agaian S. Human-visual-system-inspired underwater image quality measures. *IEEE J Ocean Eng* 2015;41(3):541–51.
- [27] Yang M, Sowmya A. An underwater color image quality evaluation metric. *IEEE Trans Image Process* 2015;24(12):6062–71.